Carbon 114 (2017) 311–316

Contents lists available at ScienceDirect

Carbon

journal homepage: www.elsevier.com/locate/carbon

All-carbon-based cathode for a true high-energy-density Li-O_2 battery

Hee-Dae Lim [a, 1], Young Soo Yun [b, 1], Se Youn Cho [c], Kyu-Young Park [a], Min Yeong Song [c], Hyoung-Joon Jin [c, *, 2], Kisuk Kang [a, **, 2]

[a] Department of Materials Science and Engineering, Seoul National University, Seoul 151-742, Republic of Korea
[b] Department of Chemical Engineering, Kangwon National University, Samcheok 245-711, Republic of Korea
[c] Department of Polymer Science and Engineering, Inha University, Incheon 402-751, Republic of Korea

ARTICLE INFO

Article history:
Received 15 August 2016
Received in revised form
29 November 2016
Accepted 3 December 2016
Available online 7 December 2016

Keywords:
Silk
Pyroprotein
Carbon mesh
Air electrode
Current collector
Li-O_2 battery

ABSTRACT

Li-O_2 batteries have a high theoretical energy density; however, their current cathode system based on a heavy metal framework strikingly diminishes their real energy density. Herein, we report the fabrication of all-carbon-based cathodes composed of conventional active carbon and a carbon mesh (CM) framework produced from waste silk fabric by simple pyrolysis. CM frameworks show a high electrical conductivity of ~150 S cm^{-1}, good tensile strength of 34.1 ± 5.2 MPa, and a Young's modulus of 4.03 ± 0.7 GPa, as well as a well-ventilated ordered macroporous structure. These all-carbon-based cathodes exhibit stable cycling and high energy densities of ~2600 Wh kg^{-1} based on total electrode weight, which are 4–15 times higher than those of conventional air cathodes.

1. Introduction

The environmental impact of fossil fuels along with the rising demand for high-energy storage systems have driven researchers to develop renewable and eco-friendly power sources. Unfortunately, Li-ion batteries (LIBs), the predominant power source so far, are not suitable for large-scale applications such as electric vehicles (EVs) and hybrid electric vehicles (HEVs) owing to their low energy density. Therefore, further research has examined alternative power sources with high energy density and renewable green chemistry. Among several candidates, the Li-O_2 battery has attracted considerable attention due to its ability to utilize atmospheric oxygen [1–7]. The direct reaction between Li ions and O_2 ($2Li^+ + O_2 + 2e^- \rightarrow Li_2O_2$) does not require heavy transition metal hosts and is therefore attractive for large-scale energy storage systems [8–10].

The in situ formation and decomposition of the solid discharge product, lithium peroxide (Li_2O_2), during electrochemical charge and discharge is a unique characteristic of Li-O_2 batteries [11–13]. The discharge product is an insulator and inhibits rapidly progress of occurring reaction. This is an important consideration in the selection and production of cathode containing an active carbon material with high specific surface area. Accordingly, a porous cathode with a well-ventilated framework is required to accommodate the solid discharge products and avoid early clogging of the air cathode. To accomplish this, robust electrode designs with hierarchical pore structure have been developed, utilizing active carbon and a metal mesh substrate such as nickel, aluminum, or stainless steel [14–16]. However, the use of heavy metals can cause a serious loss in the overall energy density of Li-O_2 batteries. Most reported energy densities of Li-O_2 batteries are significantly overestimated, since they are calculated based on the weight of active carbons only. Therefore, a lighter, more robust, and well-ventilated framework substitute for the heavy metal mesh would greatly improve future high-energy-density Li-O_2 batteries. Nevertheless, this issue remains unsolved in the Li-O_2 battery society.

Carbon-based compounds are valuable alternative substrates for Li-O_2 batteries, due to their light weight, high conductivity, chemical and thermal stability, good mechanical properties, and affordability. Although conventional carbon papers have recently been adopted, a more ordered macroporous structure and a lighter framework are required when using these materials as a substrate

* Corresponding author.
** Corresponding author.
E-mail addresses: hjjin@inha.ac.kr (H.-J. Jin), matlgen1@snu.ac.kr (K. Kang).
[1] Hee-Dae Lim, Young Soo Yun contributed equally to this work.
[2] Hyoung-Joon Jin, Kisuk Kang contributed equally to this work.

http://dx.doi.org/10.1016/j.carbon.2016.12.014
0008-6223/

for the Li-O_2 battery cathode. Moreover, considering scalable production, the development of a simpler eco-friendly process with unique material characteristics is also important.

This study highlights the development of a high-energy-density Li-O_2 battery using all-carbon-based cathodes composed of carbonaceous meshes (CMs) and active carbons such as Ketjen black (KB) and purified carbon nanotubes (*p*-CNTs). CMs have a hierarchical pore structure and are formed by simple heating of waste silk fabric (WSF). This fabric is about 20 times lighter than a conventional metal mesh, and heating greatly enhances its specific energy density. CMs possess favorable mechanical properties as well as chemical and thermal stability, achieving good electrochemical performance of all-carbon-based cathodes for Li-O_2 batteries.

2. Experimental

2.1. Fabrication of CMs

Mesh organdy silk fabric was purchased from the Dongdaemun Shopping Complex in South Korea and boiled for 30 min in a 0.02 M aqueous solution of Na_2CO_3 (99%; OCI Co.). The fabric was thoroughly rinsed with deionized water to extract the impurities. After drying at room temperature for 72 h, the silk fabric was carbonized in a furnace at temperatures from 800 to 1600 °C. After washed with ethanol and followed by deionized water, to remove residual water, the samples were subsequently heated to 150 °C for 2 h at a rate of 5 °C min^{-1}, followed by a 2 h at the desired temperature under an argon atmosphere (minimum purity: 99.9990%; gas flow: 100 cm^3 min^{-1}). The resulting CMs were stored in a desiccator.

2.2. Preparation of p-CNTs

Commercial CNTs (CM-250, Hanwha Chemical, Korea) were immersed in 60% HNO_3 solution at 60 °C and stirred for 3 h. After vacuum filtration, the samples were washed with deionized water until neutral pH. The obtained CNTs were subsequently dried in an oven at 30 °C and then heated at a rate of 5 °C min^{-1}, followed by a 2 h isotherm at 1000 °C under an argon atmosphere (minimum purity: 99.9990%; gas flow: 100 cm^3 min^{-1}). The resulting *p*-CNTs were stored in a desiccator.

2.3. Cell configurations

The air electrode was composed of KB (EC 600JD) or *p*-CNTs with Kynar 2801 binder (8:2 wt ratio) on several types of current collectors. The KB and binder were mixed into a paste using a mortar and pestle, rolled to uniform thickness, and dried in a convection oven at 120 °C. The *p*-CNTs and binder were prepared using the same method; however, the mixture was dried at −50 °C and 0.0045 mbar using a lyophilizer for 48 h after freezing at −196 °C. Ni mesh, Ni foam, and Al mesh (Nillaco Corp., 12.7 mm diameter) were used as current collectors. A Swagelok-type Li-air cell was prepared in the following sequence: Li metal anode, separator (Whatman GF/D microfiber paper), and the prepared air cathode. Lithium bis(trifluoromethane)sulfonimide (LiTFSI, 1 M) in tetraethylene glycol dimethyl ether (TEGDME) was used as the electrolyte, and all cells were tested in an atmosphere of pure oxygen (770 Torr outer pressure) using a potentio-galvanostat (WonA Tech, WBCS 3000, Korea) at a current density of 0.2 mA cm^{-2}. All electrode components were fully soaked with electrolyte, and the cells were relaxed for 0.5 h before testing. The cyclability of the CM-KB electrode was evaluated with a capacity limit of 0.5 mAh at a constant rate of 0.2 mA cm^{-2}.

2.4. Characterization

The morphologies of CMs and *p*-CNTs were examined by field-emission scanning electron microscopy (FE-SEM; Philips, XL 30 FEG, Eindhoven, Netherlands) and field-emission transmission electron microscopy (FE-TEM; JEOL, JEM2100F, Japan). Raman spectra were recorded using a linearly polarized continuous-wave laser (wavelength: 514.5 nm; 2.41 eV; power: 16 mW). The laser beam was focused by a ×100 objective lens, resulting in a spot of ca. 1 μm diameter. An acquisition time of 10 s and three scans were used to collect each spectrum. X-ray diffraction (XRD; Rigaku DMAX 2500) was carried out using Cu K_α radiation ($\lambda = 0.154$ nm) at 40 kV and 100 mA. X-ray photoelectron spectroscopy (XPS; PHI 5700 ESCA, Chanhassen, MN, USA) with monochromatic Al K_α radiation ($h\nu = 1486.6$ eV) was used to examine the chemical composition of the samples. The mechanical properties were tested using an Instron 4665 ultimate tensile testing machine (UTM) at 20 °C and 30% humidity. The porosity of *p*-CNTs was analyzed using nitrogen adsorption and desorption isotherms obtained based on the surface area, using a porosimetry analyzer (ASAP 2020, Micromeritics, USA) at −196 °C.

3. Results and discussion

The schematic diagram in Fig. S1 shows that the metal current collector (the substrate of the air cathode) has the highest weight proportion (over 82 wt%) among all key components (including Li metal, electrolyte, separator, binder, and active material) of a conventional laboratory-scale single Li-O_2 cell (See Table S1 for more specific information). Nevertheless, a well-ventilated and ordered macroporous structure, along with hardness and electrochemical stability of the metal current collector, is necessary to stably accommodate the solid Li_2O_2 discharge products during cycling. In this respect, to substitute the heavy substrate with a light component, we designed a new light substrate (with a structure similar to that of the conventional metal current collector) using waste silk fabric (WSF). WSFs are well-organized by several threads and exhibit a macroporous structure [Fig. 1(a)]. Simple heating transformed WSFs into a carbonaceous material called pyroprotein [17,18], and their morphology was well-maintained even after heating at 1400 °C, with a small shrinkage [Fig. 1(b–d)]. The pore size and structure of CMs were similar to those of the conventional Ni mesh [Fig. S2]. However, it should be noted that the CM area density (2.5 mg cm^{-2}) was ~27 times smaller than that of conventional metal meshes (Ni mesh, 68.5 mg cm^{-2}).

CMs have poorly developed graphitic structures with 1~2-nm L_c and 2~4-nm L_a, calculated from XRD patterns and Raman spectra, respectively, with scarcely grown microstructures due to the increase of pyrolysis temperatures [Fig. 2(a) and (b)]. Increasing the heating temperature from 800 to 1600 °C caused the *D* and *G* bands in the Raman spectra of CMs to become narrower due to the development of sp^2-conjugated carbon structures. Furthermore, the electroconductivity of CMs increased with pyrolysis temperature due to the hexagonal carbon planes being more ordered [Fig. 3]. CM-800 and CM-1000 exhibited electroconductivities of ~0.4 and ~2.5 S cm^{-1}, respectively. The conductivity was remarkably increased for the heating temperature range of 1000–1200 °C, and CM-1200, CM-1400, and CM-1600 showed high electroconductivities of ~60, ~150, and ~300 S cm^{-1}, respectively [Fig. 3].

The mechanical properties of CMs also changed with increasing temperatures [Table 1]. The CM tensile strength and Young's modulus increased dramatically between 1000 and 1200 °C and between 1200 and 1400 °C, respectively. As a result, CMs prepared

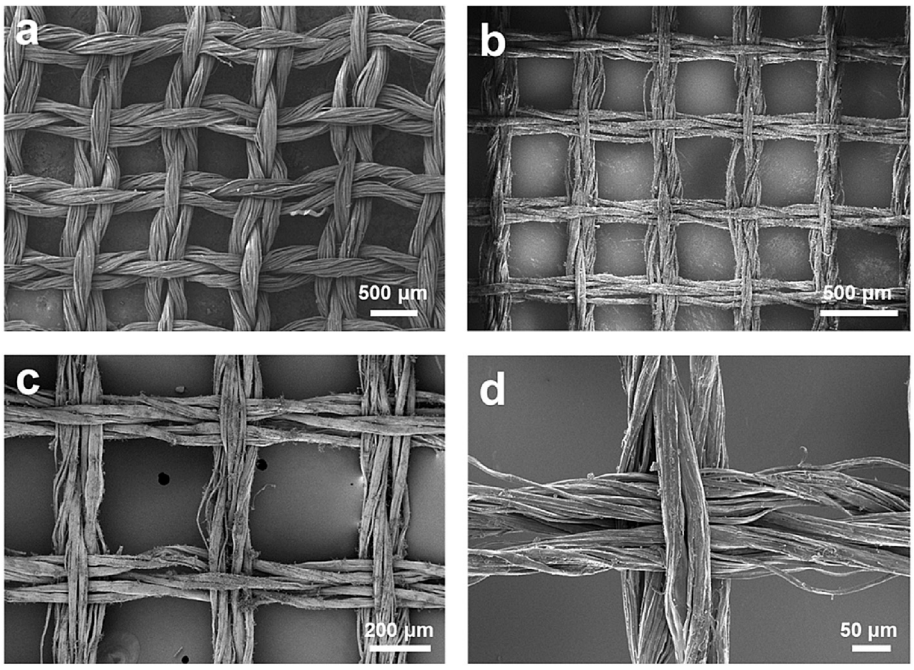

Fig. 1. FE-SEM images of (a) WSF and (b–d) CM-1400 at different magnifications.

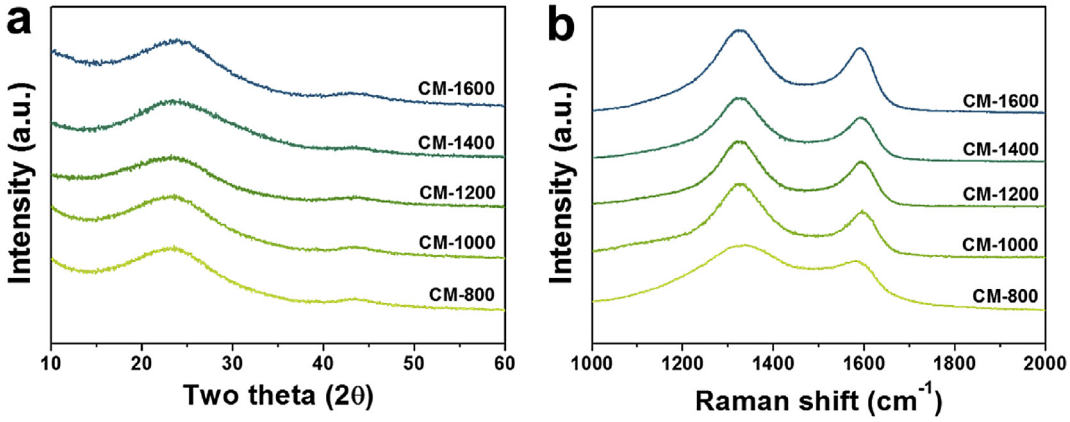

Fig. 2. (a) XRD data and (b) Raman spectra of CMs heat-treated at different temperatures. (A colour version of this figure can be viewed online.)

at 1400 °C (CM-1400) exhibited optimal mechanical properties (tensile strength of 34.1 ± 5.2 MPa and Young's modulus of 4.03 ± 0.7 GPa). The XPS C 1*s* spectrum of CM-1400 [Fig. 4(a)] showed several distinct peaks of C–O and C–N bonds (centered at 285.9 eV) and of the C(=O)O bond (centered at 288.1 eV), along with the main C–C bond peak centered at 284.7 eV. Moreover, two distinct C=O peaks centered at 531.2 eV a C–O peak centered at 532.9 eV were observed in the XPS O 1*s* spectrum [Fig. 4(b)]. The XPS N 1*s* spectrum [Fig. 4(c)] showed peaks due to pyridinic (centered at 397.7 eV) and quaternary N atoms (centered at 400.7 eV). The C/O and C/N ratios were 10.5 and 15.7, respectively. The high nitrogen content may be a major contributor to the electrical properties of CM-1400, leading to a high electroconductivity of ~150 S cm^{-1}, as shown in Fig. 3 [16,17]. In addition, another merit of CM-1400 is its improved chemical and thermal stability compared to conventional metal substrates. Furthermore, its low cost, easy processing, and potential for large-scale production are considerable advantages for Li-O_2 battery cathode applications.

The all-carbon-based cathode was prepared based on CM-1400 using conventional active carbon (KB). The robust self-standing CMs with 1.27 cm in diameter are shown in Fig. 5(a), and the Li-O_2 cell electrode composed of KB and CM-1400 (CM-KB) is shown in Fig. 5(b). The self-standing CMs are stable in the TEGDME electrolyte [Fig. S3], and KB is well attached to the carbon framework and stably maintained during the overall cell assembly process. The electrochemical properties of the CM-KB Li-O_2 cell electrode are demonstrated in Fig. 5(c). The corresponding reversible discharge-charge cycles prove that this lighter CM-KB system effectively achieves a performance similar to that of a conventional Ni mesh-based system (Ni-KB). The profiles are similar to those previously reported for KB electrodes [19,20], implying the formation/decomposition of Li_2O_2. Stable and reversible cycling was observed over 15 cycles, which is comparable to the conventional electrode using a metal mesh framework [Fig. 5(d)]. The major discharge product was Li_2O_2, with a small amount of lithium hydroxide (LiOH) detected after the first discharge, as shown in Fig. 5(e), which is similar to the previous report employing a metal substrate

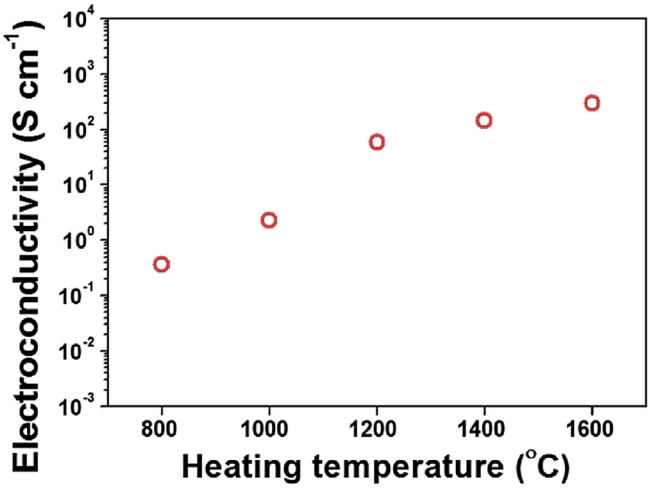

Fig. 3. Change of electroconductivities of CMs according to heating temperature. (A colour version of this figure can be viewed online.)

Table 1
Mechanical properties of CMs obtained at different heating temperatures.

Sample	Young's modulus (GPa)	Tensile strength (MPa)	Strain
CM-800	2.1 ± 0.1	17.3 ± 1.8	0.95 ± 0.06
CM-1000	2.2 ± 0.1	24.9 ± 2.2	0.82 ± 0.05
CM-1200	2.3 ± 0.1	38.3 ± 4.8	0.85 ± 0.07
CM-1400	4.0 ± 0.7	34.1 ± 5.2	0.56 ± 0.04
CM-1600	4.4 ± 0.1	32.8 ± 2.3	0.51 ± 0.04

[21,22]. In addition, small amount of by-product such as Li_2CO_3 in an amorphous structure could be formed simultaneously with the major discharge products, which was demonstrated in previous reports [23,24]. Fig. 5(f) shows an FE-SEM image of the air electrode after charge/discharge cycling. The overall CM-KB morphology was almost similar to that of the as-prepared electrode, indicating that CMs are quite sustainable and stable during cycling. On the other hand, commercial carbon papers used as substrates for Li-O_2 cells were easily clogged with solid discharge products and quickly lost their original morphology, as shown in the inset of Fig. 5(f). This is attributed to their unordered pore structure with relatively small pores, which can easily make the electrode surface clogged with solid Li_2O_2 during discharge [Fig. S4].

Although CM-KB functions effectively in Li-O_2 cells, its cyclability is still quite low and needs to be improved. Low cyclability is the prevailing problem of current Li-O_2 batteries and is attributed to the reaction between bulk carbon (*i.e.,* KB) and the electrolyte deteriorated at high potential during charging [20,25,26]. To solve these problems, we used *p*-CNTs with high crystallinity and aspect ratio as an active material [Fig. S5] and employed a soluble LiI catalyst (proven to be effective for the decomposition of Li_2O_2) to decrease charge polarization [27–29]. Furthermore, to create a stable hierarchical pore structure, a freeze-drying method was used instead of oven drying. As shown in Fig. 6(a) and (b), the loosely packed *p*-CNTs covered the entire CM area, which exhibited numerous pores of different sizes. The cyclability of Li-O_2 cells consisting of the all-carbon-based electrode (CM-CNT) and LiI catalyst was demonstrated to be increased to > 40 cycles, as shown in Fig. 6(c). The charge polarization was decreased by using the liquid catalyst, resulting in a small overpotential gap between the discharge and charge processes, shown in the inset of Fig. 6(c). This further enhancement of electrochemical properties demonstrates that CM-CNT can potentially be utilized in Li-O_2 batteries.

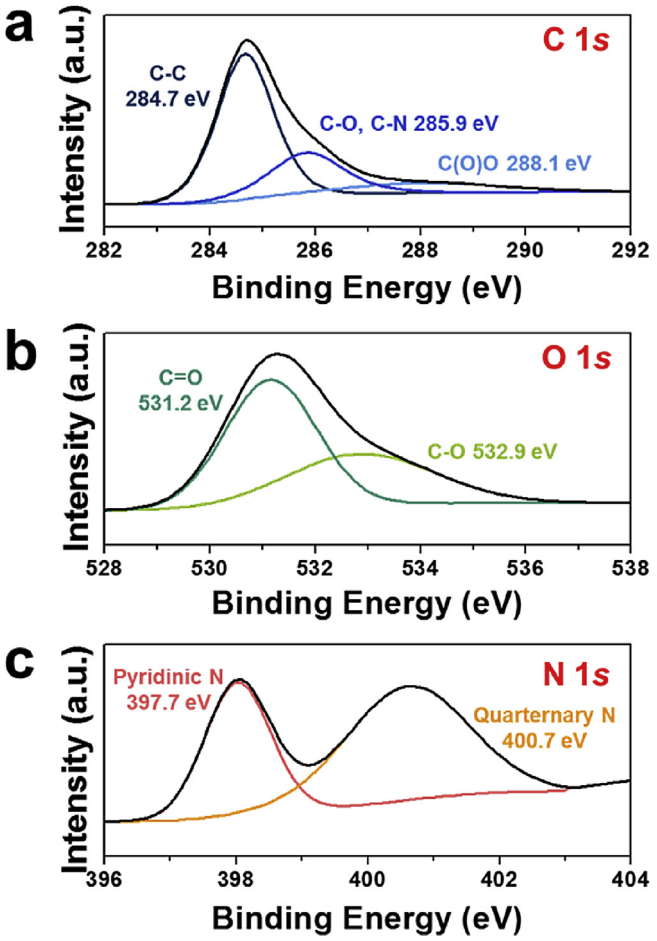

Fig. 4. (a) C 1*s*, (b) O 1*s*, and (c) N 1*s* XPS spectra of CM-1400. (A colour version of this figure can be viewed online.)

The specific capacities and energy densities of different cathodes are compared in Fig. 6(d). Considering the active carbon weight only, the specific capacity of mesh-type cathodes seems to be extremely high (~3500 mAh g^{-1}) and consistent, as denoted by the orange bars in Fig. 6(d). However, the specific capacities based on total electrode weight (blue bars) are much lower. The real specific capacities of Li-O_2 batteries based on Ni mesh, carbon paper (CP), Al mesh, and Ni foam were only 56, 130, 141, and 264 mAh g^{-1}, respectively, not much higher than that of the Li-ion battery. In contrast, the all-carbon-based cathodes can deliver a capacity of over 1000 mAh g^{-1}, even when calculated based on the total electrode weight, which corresponds to a high energy density of 2616 Wh kg^{-1}. This value is 4–15 times higher than that of other cathodes. Full discharge profiles of the different cathodes, based on total electrode weight, show the differences in real capacities more clearly [Fig. S6]. Although CP is lighter than other metal meshes, it delivers a small capacity due to an unordered framework with relatively small pores, which leads to premature surface clogging by solid discharge products [Fig. S4]. This clearly demonstrates that the use of CMs can dramatically improve the true energy density of Li-O_2 batteries while maintaining the mechanical and chemical stability of the substrate.

4. Conclusion

In this study, simple heating of WSF afforded light and sustainable CMs with well-ventilated macroporous structures for use

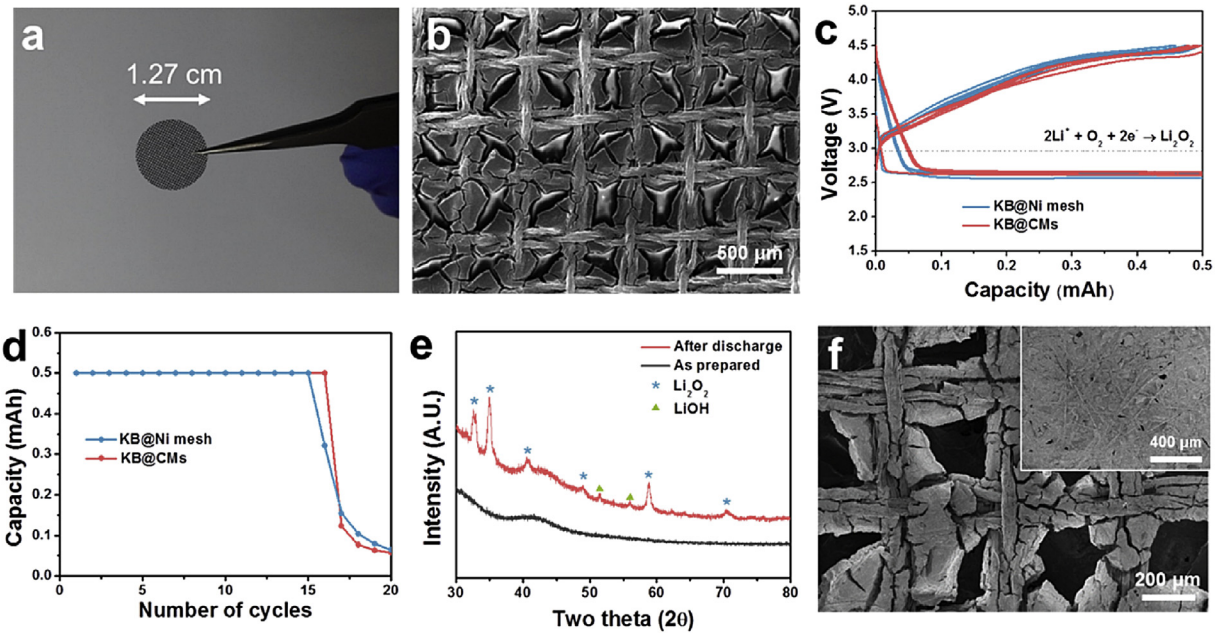

Fig. 5. (a) Image of the self-standing carbon mesh substrate. (b) FE-SEM image of the air cathode composed of KB carbon and CM substrate. (c) Charge/discharge profiles of the CM-KB electrode for 10 cycles, at up to 500 mAh g^{-1} and a constant rate of 0.2 mA cm^{-2}. The dotted line shows the theoretical potential of Li_2O_2 formation (2.96 V). (d) Comparison of Li-O_2 cell cyclability using CM-KB and Ni-KB electrodes. (e) XRD spectrum of the CM-KB electrode obtained after discharge. (f) FE-SEM image of the CM-KB electrode (inset: carbon paper electrode) after cycling. (A colour version of this figure can be viewed online.)

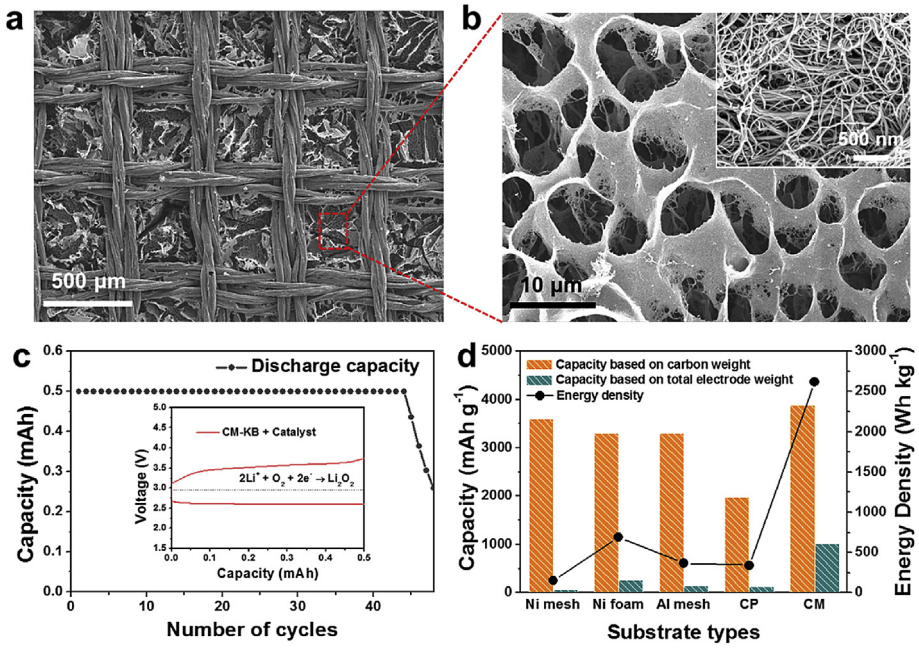

Fig. 6. (a),(b) FE-SEM image of the all-carbon-based electrode with CNTs and carbon mesh with different magnification. (c) The charge/discharge profiles of Li-O_2 cells with the all-carbon-based electrode at a constant rate of 0.2 mA cm^{-2} and (inset) cyclability with a limited capacity at 0.5 mAh. (d) Capacity and energy density comparison according to substrate type. (A colour version of this figure can be viewed online.)

in novel all-carbon-based electrodes for Li-O_2 batteries. CM-1400 showed a high electrical conductivity of ~150 S cm^{-1}, a tensile strength of 34.1 ± 5.2 MPa, and a Young's modulus of 4.03 ± 0.7 GPa. The all-carbon-based CM cathode could deliver a specific capacity of ~1000 mAh g^{-1} and an energy density of ~2600 Wh kg^{-1} (4–15 times higher than the corresponding values of conventional cathodes) along with stable cycling. The substitution of the conventional heavy metal framework by a light carbon mesh is a breakthrough that can have a major impact on future large-scale production of Li-O_2 batteries.

Acknowledgments

This work was supported by the World Premier Materials grant funded by the Korea government Ministry of Trade, Industry and Energy and also supported by Basic Science Research Program

through the National Research Foundation of Korea (NRF) funded by the Ministry of Education (NRF-2016R1A2B4009601).

Appendix A. Supplementary data

Supplementary data related to this article can be found at http://dx.doi.org/10.1016/j.carbon.2016.12.014.

References

[1] P.G. Bruce, S.A. Freunberger, L.J. Hardwick, J.-M. Tarascon, Li-O2 and Li-S batteries with high energy storage, Nat. Mater. 11 (1) (2012) 19–29.
[2] Z. Peng, S.A. Freunberger, Y. Chen, P.G. Bruce, A reversible and higher-rate Li-O2 battery, Science 337 (6094) (2012) 563–566.
[3] D. Oh, J. Qi, Y.-C. Lu, Y. Zhang, Y. Shao-Horn, A.M. Belcher, Biologically enhanced cathode design for improved capacity and cycle life for lithium-oxygen batteries, Nat. Commun. 4 (2013) 2756.
[4] F. Li, T. Zhang, H. Zhou, Challenges of non-aqueous Li-O2 batteries: electrolytes, catalysts, and anodes, Energy Environ. Sci. 6 (4) (2013) 1125–1141.
[5] J. Lu, L. Li, J.-B. Park, Y.-K. Sun, F. Wu, K. Amine, Aprotic and aqueous Li–O2 batteries, Chem. Rev. 114 (11) (2014) 5611–5640.
[6] B.G. Kim, S. Kim, H. Lee, J.W. Choi, Wisdom from the human eye: a synthetic melanin radical scavenger for improved cycle life of Li–O2 battery, Chem. Mater 26 (16) (2014) 4757–4764.
[7] J. Lu, Y.J. Lee, X. Luo, K.C. Lau, M. Asadi, H.-H. Wang, et al., A lithium–oxygen battery based on lithium superoxide, Nature 529 (2016) 377–382.
[8] B.D. Adams, C. Radtke, R. Black, M.L. Trudeau, K. Zaghib, L.F. Nazar, Current density dependence of peroxide formation in the Li-O2 battery and its effect on charge, Energy Environ. Sci. 6 (6) (2013) 1772–1778.
[9] H.-K. Lim, H.-D. Lim, K.-Y. Park, D.-H. Seo, H. Gwon, J. Hong, et al., Toward a Lithium–"Air" battery: the effect of CO2 on the chemistry of a lithium–oxygen cell, J. Am. Chem. Soc. 135 (26) (2013) 9733–9742.
[10] J.-S. Lee, S. Tai Kim, R. Cao, N.-S. Choi, M. Liu, K.T. Lee, et al., Metal–air batteries with high energy density: Li–Air versus Zn–Air, Adv. Energy Mater 1 (1) (2011) 34–50.
[11] S. Ganapathy, B.D. Adams, G. Stenou, M.S. Anastasaki, K. Goubitz, X.-F. Miao, et al., Nature of Li2O2 oxidation in a Li–O2 battery revealed by operando X-ray diffraction, J. Am. Chem. Soc. 136 (46) (2014) 16335–16344.
[12] H. Lim, E. Yilmaz, H.R. Byon, Real-time XRD studies of Li–O2 electrochemical reaction in nonaqueous lithium–oxygen battery, J. Phys. Chem. Lett. 3 (21) (2012) 3210–3215.
[13] C. Yang, R.A. Wong, M. Hong, K. Yamanaka, T. Ohta, H.R. Byon, Unexpected Li2O2 film growth on carbon nanotube electrodes with CeO2 nanoparticles in Li–O2 batteries, Nano Lett. 16 (5) (2016) 2969–2974.
[14] J. Li, H. Zhang, Y. Zhang, M. Wang, F. Zhang, H. Nie, A hierarchical porous electrode using a micron-sized honeycomb-like carbon material for high capacity lithium-oxygen batteries, Nanoscale 5 (11) (2013) 4647–4651.
[15] H.-D. Lim, K.-Y. Park, H. Song, E.Y. Jang, H. Gwon, J. Kim, et al., Enhanced power and rechargeability of a Li–O2 battery based on a hierarchical-fibril CNT electrode, Adv. Mater. 25 (9) (2013) 1348–1352.
[16] S.H. Oh, R. Black, E. Pomerantseva, J.-H. Lee, L.F. Nazar, Synthesis of a metallic mesoporous pyrochlore as a catalyst for lithium–O2 batteries, Nat. Chem. 4 (12) (2012) 1004–1010.
[17] S.Y. Cho, Y.S. Yun, S. Lee, D. Jang, K.-Y. Park, J.K. Kim, et al., Carbonization of a stable [beta]-sheet-rich silk protein into a pseudographitic pyroprotein, Nat. Commun. 6 (2015) 7145.
[18] Y.S. Yun, S.Y. Cho, J. Shim, B.H. Kim, S.-J. Chang, S.J. Baek, et al., Microporous carbon nanoplates from regenerated silk proteins for supercapacitors, Adv. Mater 25 (14) (2013) 1993–1998.
[19] S.H. Oh, L.F. Nazar, Oxide catalysts for rechargeable high-capacity Li–O2 batteries, Adv. Energy Mater 2 (7) (2012) 903–910.
[20] H.-D. Lim, K.-Y. Park, H. Gwon, J. Hong, H. Kim, K. Kang, The potential for long-term operation of a lithium-oxygen battery using a non-carbonate-based electrolyte, Chem. Commun. 48 (67) (2012) 8374–8376.
[21] R. Black, S.H. Oh, J.-H. Lee, T. Yim, B. Adams, L.F. Nazar, Screening for superoxide reactivity in Li-O2 batteries: effect on Li2O2/LiOH crystallization, J. Am. Chem. Soc. 134 (6) (2012) 2902–2905.
[22] J.-H. Lee, R. Black, G. Popov, E. Pomerantseva, F. Nan, G.A. Botton, et al., The role of vacancies and defects in Na0.44MnO2 nanowire catalysts for lithium-oxygen batteries, Energy Environ. Sci. 5 (11) (2012) 9558–9565.
[23] C. Li, Z. Guo, Y. Pang, Y. Sun, X. Su, Y.-G. Wang, et al., Three-dimensional ordered macroporous FePO4 as high efficient catalyst for rechargeable Li-O2 batteries, ACS Appl. Mater. Interfaces 8 (46) (2016) 31638–31645.
[24] B.D. McCloskey, A. Speidel, R. Scheffler, D.C. Miller, V. Viswanathan, J.S. Hummelshøj, et al., Twin problems of interfacial carbonate formation in nonaqueous Li–O2 batteries, J. Phys. Chem. Lett. 3 (8) (2012) 997–1001.
[25] M.M. Ottakam Thotiyl, S.A. Freunberger, Z. Peng, P.G. Bruce, The Carbon Electrode in Nonaqueous Li–O2 Cells, J. Am. Chem. Soc. 135 (1) (2012) 494–500.
[26] S.R. Gowda, A. Brunet, G.M. Wallraff, B.D. McCloskey, Implications of CO2 contamination in rechargeable nonaqueous Li–O2 batteries, J. Phys. Chem. Lett. 4 (2) (2013) 276–279.
[27] H.-D. Lim, H. Song, J. Kim, H. Gwon, Y. Bae, K.-Y. Park, et al., Superior rechargeability and efficiency of lithium–oxygen batteries: hierarchical air electrode architecture combined with a soluble catalyst, Angew. Chem. Int. Ed. 53 (15) (2014) 3926–3931.
[28] M. Yu, X. Ren, L. Ma, Y. Wu, Integrating a redox-coupled dye-sensitized photoelectrode into a lithium–oxygen battery for photoassisted charging, Nat. Commun. 5 (2014) 5111.
[29] T.H. Yoon, Y.J. Park, New strategy toward enhanced air electrode for Li-air batteries: apply a polydopamine coating and dissolved catalyst, RSC Adv. 4 (34) (2014) 17434–17442.